

Magnetohydrodynamic jets from different magnetic field configurations

Christian Fendt

Abstract Using axisymmetric MHD simulations we investigate how the overall jet formation is affected by a variation in the disk magnetic flux profile and/or the existence of a central stellar magnetosphere. Our simulations evolve from an initial, hydrostatic equilibrium state in a force-free magnetic field configuration. We find a unique relation between the collimation degree and the disk wind magnetization power law exponent. The collimation degree decreases for steeper disk magnetic field profiles. Highly collimated outflows resulting from a flat profile tend to be unsteady. We further consider a magnetic field superposed of a stellar dipole and a disk field in parallel or anti-parallel alignment. Both stellar and disk wind may evolve in a pair of outflows, however, a reasonably strong disk wind component is essential for jet collimation. Strong flares may lead to a sudden change in mass flux by a factor two. We hypothesize that such flares may eventually trigger jet knots.

1 Jets as collimated MHD flows

Astrophysical jets are launched by magnetohydrodynamic (MHD) processes in the close vicinity of the central object – an accretion disk surrounding a protostar or a compact object [1, 2, 9, 20, 21, 24]. Numerical simulations of MHD jet formation are essential for our understanding of the physical processes involved. In general, simulations may be distinguished in those taking into account the evolution of the disk structure and others considering the disk surface as a fixed-in-time boundary condition for the jet. The first approach allows to directly investigate the mechanism lifting matter from the disk into the outflow [3, 10, 11, 14, 17, 18, 22, 24] This approach is computationally expensive and still somewhat limited by spatial and time resolution. In order to study the acceleration and collimation of a disk/stellar

Christian Fendt
Max Planck Institute for Astronomy, Königstuhl 17, D-69117 Heidelberg, e-mail:
fendt@mpia.de

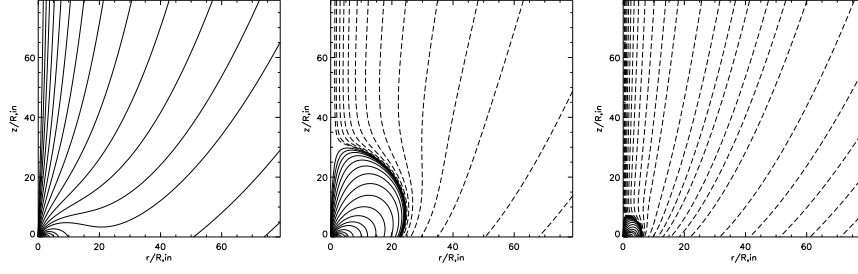


Fig. 1 Example initial magnetic field distributions (poloidal magnetic field lines). Full and dashed lines indicate the direction of magnetic flux. Magnetic field parameters: $\Psi_{0,\text{disk}} = 0.01; 0.01; 0.1$; resp. $\Psi_{0,z} = 5; 5; 3$ (from left to right). From [5].

wind it is essential to follow the dynamical evolution for i) very long time ii) on a sufficiently large grid with iii) appropriate resolution. For such a goal, the second approach is better suited [4-7, 12, 13, 15, 19, 25], allowing as well for parameter studies. The case of superposed stellar/disk magnetic field is rarely treated in simulations, still, the first model was discussed already in [23]. Simulations of a dipole with aligned vertical disk field are presented by [16, 18]. The stellar field has important impact on the jet formation process as enhancing the magnetic flux, adding a central pressure, and providing excess angular momentum for the launching region.

2 Model setup

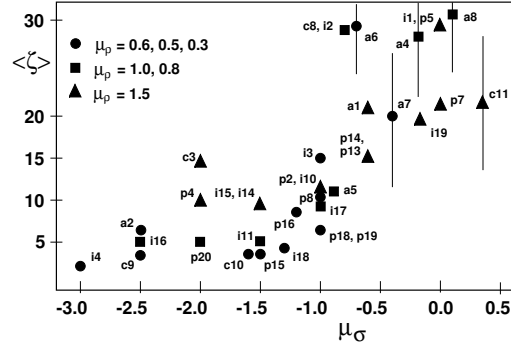
We use the ZEUS-3D MHD code extended for physical magnetic resistivity (see description in [6]). The set of MHD equations considered is the following,

$$\frac{\partial \rho}{\partial t} + \nabla \cdot (\rho \mathbf{v}) = 0; \quad \nabla \times \mathbf{B} = \frac{4\pi}{c} \mathbf{j} = \nabla \times \mathbf{B}; \quad \frac{\partial \mathbf{B}}{\partial t} - \nabla \times \mathbf{v} \times \mathbf{B} - \frac{4\pi}{c} \eta \mathbf{j} = 0 \quad (1)$$

$$\rho \frac{\partial \mathbf{u}}{\partial t} + (\mathbf{v} \cdot \nabla) \mathbf{v} + \nabla (p + p_A) + \rho \nabla \Phi - \frac{\mathbf{j} \times \mathbf{B}}{c} = 0; \quad (2)$$

with the usual notation [4-7, 19]. We do not solve the energy equation, but apply an internal energy $e = p/(\gamma - 1)$ of a polytropic gas ($\gamma = 5/3$). Turbulent Alfvénic pressure p_A allows for a "cool" corona. The turbulent magnetic diffusivity $\eta(r, z, t)$ can be related to p_A applying our toy model [6]. The $\eta = 0.01$ was chosen low and does not affect collimation. Diffusivity is, however, essential for reconnection processes. We distinguish setup *DW* (pure disk wind) and *SDW* (stellar wind plus disk wind) by choice of boundary and initial conditions. Model *DW* investigates different disk magnetic field and mass flux profiles [4]. Model *SDW* investigates the interrelation of the stellar magnetosphere with the surrounding disk jet [5].

Fig. 2 Collimation degree $\langle \zeta \rangle$ and power index of the disk wind magnetization profile μ_σ . Bars indicate simulations with time variable collimation degree (from [4]).



Boundary conditions: In setup DW we distinguish along the equatorial plane the gap region $r < 1 \Omega$ and disk region $r > 1 \Omega$. The magnetic field is fixed in time and is determined by the initial condition. We have chosen a power law, $B_p(r;0) = r^{-\mu}$, and investigate different μ . In setup SDW we further distinguish the star from $r = 0$ to 0.5 , and the gap from $r = 0.5$ to 1Ω . Co-rotation radius and inner disk radius coincide. A Keplerian disk is the boundary condition for the mass inflow from the disk surface into the corona. Matter is “injected” from the disk (and the star) with low velocity $\mathbf{v}_{\text{inj}}(r;0) = v_i v_K(r) \mathbf{B}_p / B_p$ and density $\rho_{\text{inj}}(r;0) = \eta_i \rho(r;0)$. Typically, $v_i \sim 10^{-3}$ and $\eta_i \sim 100$ for stellar and disk wind, but could be chosen differently.

Initial conditions: As initial state we prescribe a force-free magnetic field and a hydrostatic equilibrium $\rho(r;z;t=0) = (r^2 + z^2)^{-3/4}$. For model DW we calculate the initial field distribution from the disk magnetic field profile using our finite element code (see [4,8]). For model SDW the initial field is a superposed dipole plus disk field. For the disk component we apply the potential field of [6,19]. We prescribe the initial field by the magnetic flux distribution $\Psi(r;z) = \mathbf{B}_p d\mathbf{A}$,

$$\Psi(r;z) = \Psi_{0,d} \frac{1}{r} \frac{r^2}{r^2 + (z_d + z)^2} (z_d + z) + \Psi_{0,i} \frac{r^2}{(r^2 + (z_d + z)^2)^{3/2}} : \quad (3)$$

Certain field combinations are investigated, parameterized by the disk $\Psi_{0,d}$ and stellar magnetic flux $\Psi_{0,i}$ (Fig. 1).

3 Disk wind magnetization and jet collimation

Simulations of setup DW were run for different disk magnetic field profiles $B_p(r;z=0) = r^{-\mu}$ and density profiles $\rho_{\text{inj}}(r;z=0) = r^{-\mu\rho}$. In general, we find an increasing degree of collimation with decreasing slope of the disk magnetic field profile (see [4]). This seems to rule out launching models for collimated jets from a concentrated magnetic flux such as e.g. the X-wind scenario. A steep density profile leads to a higher collimation degree, which is not surprising as the mass flux is more

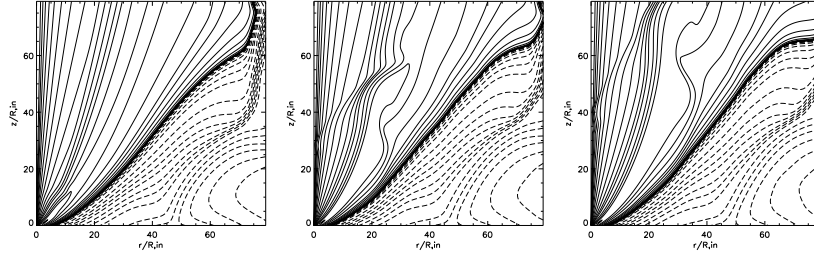


Fig. 3 Poloidal magnetic field evolution during one example flare around $t = 180$. Solid and dashed lines indicate the direction of total magnetic flux of the superposed dipolar and disk magnetic field components. Shown are time steps: 1760, 1790, 1810 (from left to right).

concentrated just by definition of the boundary condition. A physically meaningful classification taking into account both density and magnetic field can be achieved by comparing the degree of collimation degree versus disk wind *magnetization* profile, $\sigma(r; z=0) = \frac{B_p^2(r)r^4 \rho_{inj}^{-1} v_{inj}^{-1}(r) \Omega_K(r)^2}{r^{2\mu_\sigma + 1} \mu_\sigma}$, thus, $\sigma(r; z=0) = r^{2\mu_\sigma + 1} \mu_\sigma$. The resulting diagram Fig. 2 shows a convincing correlation between the magnetization power law index μ_σ and the average degree of collimation $\langle \zeta \rangle$. The width of the $(\mu_\sigma - \langle \zeta \rangle)$ -correlation is due to further differences in the parameter space.

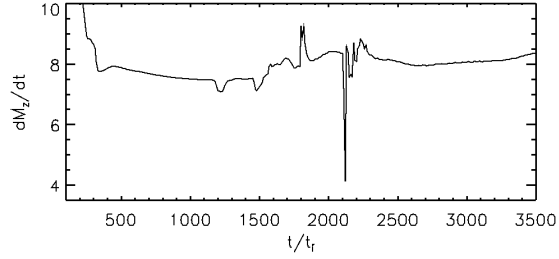
4 Jet mass flux triggered by star-disk magnetospheric flares

Simulations of setup SDW were run for aligned and anti-aligned orientation of dipole versus disk field and for different strength of both field contributions [5].

Independent of the alignment, the central dipole does not survive on the large scale. A two-component outflow emerges as stellar wind plus disk wind. For a reasonably strong disk magnetic flux a collimated jet emerges. If the overall outflow is dominated by a strong stellar outflow a low mass flux disk wind remains uncollimated. The best setup to launch a collimated jet from a star-disk magnetosphere is that of a relatively heavy disk wind and high disk magnetic flux. Stellar wind dominated simulations may give a high degree of collimation, however they collimate to too small radii. Stellar magnetic flux dominated outflows tend to stay un-collimated.

In some simulations we observe reconnection flares, similar to coronal mass ejections, typically expanding and reconnecting within 70 orbital periods of the inner disk. This is similar to [10], however, in their case reconnection is triggered by time-variation of the accretion rate. In our case the reconnection/flares seem to be triggered by the evolution of the outer disk wind. Even for our very long time-scales the outer disk outflow is still dynamically evolving, thus changing the cross-jet force equilibrium and forcing the inner structure to adjust accordingly. The flare events are accompanied by a temporal change in outflow mass flux and momentum. Figure 4 shows the mass loss rate in axial direction integrated across the jet. We see two flares

Fig. 4 Axial mass flux integrated along the upper z -boundary versus time. Note the change of mass flux of 10–50% during the flare events. High mass fluxes for $t < 500$ indicate sweeping off of the initial corona.



with a 10%-increase in the mass flux followed by a sudden decrease of mass flux by a factor of two. This behavior is also mirrored in the poloidal velocity profile.

Considering the ejection of large-scale flares and the follow-up re-configuration of outflow dynamics, we hypothesize that the origin of jet knots is triggered by such flaring events. Our time-scale for flare generation is of 1000 rotational periods and longer than the typical dynamical time at the jet base, but similar to the observed knots. The flare itself for about 30-40 inner disk rotation times.

References

1. Blandford, R., Payne, D., 1982, MNRAS **199**, 883
2. Camenzind, M.: Magnetized disk-winds and the origin of bipolar outflows. In: Klare, G. (ed) Rev. Mod. Astron. 3, p.234, Springer, Heidelberg (1990)
3. Casse, F., Keppens, R. 2002, ApJ, **581**, 988
4. Fendt, C. 2006, ApJ, **651**, 272
5. Fendt, C. 2008, ApJ, in press, arXiv:0810.4154v1 [astro-ph]
6. Fendt, C., Cemeljic, M. 2002, A&A **395**, 1045
7. Fendt, C., Elstner, D. 2000, A&A **363**, 208
8. Fendt, C., Camenzind, M., Appl, S. 1995, A&A **300**, 791
9. Ferreira, J., Dougados, C., Cabrit, S. 2006, A&A **453**, 785
10. Goodson, A., Winglee, R., Böhm, K. 1997, ApJ **489**, 199
11. Hayashi, M., Shibata, K., Matsumoto, R. 1996, ApJ **468**, L37
12. Kigure, H., Shibata, K. 2005, ApJ **634**, 879
13. Krasnopolsky, R., Li, Z.-Y., Blandford, R. 1999, ApJ **526**, 631
14. Kudoh, T., Matsumoto, R., Shibata, K. 1998, ApJ **508**, 186
15. Matsakos, T., Tsinganos, K., Vlahakis, N., Massaglia, S., Mignone, A., Trussoni, E. 2008, A&A **477**, 521
16. Matt, S., Goodson, A., Winglee, R., Böhm, K.-H. 2002, ApJ **574**, 232
17. Meliani, Z., Casse, F., Sauty, C. 2007, A&A **460**, 1
18. Miller, K., Stone, J. 1997, ApJ **489**, 890
19. Ouyed, R., Pudritz, R., 1997, ApJ **482**, 712
20. Pudritz, R., Norman, C. 1983, ApJ **274**, 677
21. Pudritz, R., Ouyed, R., Fendt, C., Brandenburg, A.: Disk Winds, Jets, and Outflows: Theoretical and Computational Foundations. In: Reipurth, B., Jewitt, D., Keil, K. (ed) Protostars & Planets V, p.277, University of Arizona Press, Tucson (2007)
22. Romanova, M., Ustyugova, G., Koldoba, A., Lovelace, R. 2002, ApJ **578**, 420
23. Uchida, Y., Low, B. 1981, Journal of Astroph. and Astron. **2**, 405

- 24. Uchida, Y., Shibata, K. 1984, PASJ **36**, 105
- 25. Ustyugova, G., Koldoba, A., Romanova, M., Chechetkin, V., Lovelace, R. 1995, ApJ **439**, L39